

Precision Loading and Delivery of Molecular Cargo by Size-Controlled Coacervation of Gold Nanoparticles Functionalized with Elastin-Like Peptides

Yifeng Cai,¹ Nada Y. Naser,¹ Jinrong Ma² and François Baneyx^{1,2*}

Department of Chemical Engineering,¹ and Molecular Engineering and Sciences Institute,² University of Washington, Seattle, WA, USA

* Corresponding author: baneyx@uw.edu

Keywords: *ELP, self-assembly, stimuli-responsive systems, reconfiguration, drug delivery*

Abstract

Thermoresponsive elastin-like peptides (ELPs) have been extensively investigated in biotechnology and medicine, but little attention has been paid to the process by which coacervation causes ELP-decorated particles to aggregate. Using gold nanoparticles (AuNPs) functionalized with a 96-repeat of a cysteine-terminated VPGVG sequence (V96-Cys), we show that the size of the clusters that reversibly form above the ELP transition temperature (T_t) can be finely controlled in the 250 to 930 nm range by specifying the concentration of free V96-Cys in solution and using AuNPs of different sizes. We further find that the localized surface plasmon resonance peak of the embedded AuNPs progressively redshifts with cluster size, likely due to an increase in particle-particle contacts. We exploit this fine control over size to homogeneously load precise amounts of the dye Nile Red and the antibiotic Tetracycline into clusters of different hydrodynamic diameters, and deliver cargos near-quantitatively by deconstructing the aggregates below T_t . Beyond establishing a key role for free ELP in the agglomeration of ELP-functionalized particles, our results provide a path for thermally-controlled delivery of precise quantities of molecular cargo. This capability might prove useful in combination photothermal therapies and theranostics applications, and to trigger spatially and temporally uniform responses from biological, electronic, or optical systems.

Introduction

Stimuli-responsive nanomaterials undergo changes in structure and properties when environmental conditions are altered through the application of stimuli such as light,^{1,2} temperature,^{3,4} solution pH,^{5,6} electric,^{7,8} or magnetic fields.⁹ Interest in these materials remains exceptionally high owing to their potential in advanced sensing,^{10,11} catalysis,¹² and drug delivery.^{13,14} Heat-responsive architectures comprising gold nanoparticles (AuNPs) have been especially popular in these application fields^{15–20} owing to the fact that they exhibit unique size and shape-dependent optical and electronic properties^{21,22} and are easily decorated with thermoresponsive polymers via ligand exchange.²³

For many years, the polymer of choice was the venerable poly(*N*-isopropylacrylamide) (PNIPAm), a macromolecule that exhibits lower critical solution temperature (LCST) behavior and phase segregates in water above a phase transition temperature (T_t) whose value is modulated by polymer concentration and solution conditions.^{24–27} Thermoresponsive biopolymers such as elastin-like peptides (ELPs) have progressively supplanted PNIPAm in the biomedical space because they have the additional advantages of monodispersity and biocompatibility, and because their T_t and properties can be tailored and enhanced by genetic engineering.^{28–34} A significant body of work has focused on the functionalization of AuNPs with ELPs and on the properties and applications of these composites.^{35–39} For example, Rege and coworkers have showed that gold nanorods decorated with engineered ELPs undergo a reversible phase transition upon near-infrared light illumination, and support the hyperthermal treatment of cancer cells and the photothermal release of chemotherapeutics.^{40,41} Other groups have expanded on the use of ELP-AuNP conjugates for photothermal therapies.^{42,43} For example, Gao and coworkers have shown that ELP-AuNPs are injectable into tumors to form AuNP assemblies

as novel intelligent theranostic agents, enabling in vivo multimodal imaging and photothermal therapy of cancer.⁴⁴ However, little attention has been paid to the process through which ELP phase segregation (also referred to as coacervation) drives the reversible clustering of AuNPs, and to the exploitation of this process to control the properties and function of the clusters.

Inspired by Scherman and colleagues, who noted that the presence of free PNIPAm in solutions of PNIPAm-coated AuNPs was the primary driving force for aggregate formation above T_t ,⁴⁵ we show here that it is possible to achieve a fine control over the size of clusters that are dynamically assembled from individual ELP-functionalized AuNPs by manipulating the amount of free ELP in solution. We exploit this finding for precision loading and delivery of small molecule cargos that include the dye Nile Red (NR) and the antibiotic tetracycline (TC).

Experimental

DNA manipulation and protein purification

Plasmid pET25b(+)-ELP(V96) which encodes a 96-repeat of the VPGVG sequence terminated by a Tyr residue⁴⁶ was obtained from Addgene. The C-terminal Tyr was converted to Cys by site-directed mutagenesis, and the resulting plasmid, pET25(+)-ELP(V96)-Cys, was introduced into *E. coli* BL21(DE3) cells. Overnight cultures (5 mL) were used to inoculate 500 mL of Terrific Broth (TB) supplemented with 50 µg/mL carbenicillin at a 1:100 dilution and cells were grown with shaking at 200 rpm for 24 hours at 37°C. Cells were harvested by centrifugation at 4,000g at 4°C for 20 minutes and the pellet was frozen at -20°C or directly resuspended in 20 mL of 20 mM of Tris-HCl, pH 7.5 for purification. Cells were placed on ice and lysed by two cycles of sonication on a Fisherbrand Sonic Dismembrator with each cycle consisting of 10 seconds on and 20 seconds off at 30% amplification for

9 minutes. Lysates were centrifuged at 10,000g at 4 °C for 20 minutes to remove insoluble debris. The supernatant was supplemented with 1 mL of 10 v/v% polyethylenimine (PEI) in DI H₂O, incubated on ice for 10 minutes, and centrifuged at 10,000g and 4 °C for 20 minutes to remove precipitated nucleic acids. The V96-Cys protein was purified by inverse transition cycling (ITC) as described⁴⁷. The final resuspension was in 15 mL of DI H₂O at a final concentration of 80 to 85 μM, as determined by 205 nm absorbance measurements⁴⁸ on a NanoDrop One Microvolume UV-Vis Spectrophotometer (Thermo Scientific). Purity was greater than 95% as judged by silver-stained SDS-PAGE analysis (**Fig. S1**).

Preparation of V96-Cys-functionalized AuNP samples

Citrate-capped AuNP 60 nm or 20 nm in nominal size (64 nm and 25 nm in hydrodynamic diameter; **Fig. 1B** and **Fig. S2**) and dispersed in DI H₂O were purchased from BBI Solutions (Portland, ME). V96-Cys-functionalized AuNPs were prepared by mixing 200 μL of an 80 μM protein stock with 1 mL of AuNP solution in a 2 mL glass vial. This concentration of V96-Cys (13.3 μM) was necessary to preserve colloidal stability during the citrate-ELP ligand exchange step (**Fig. S3**). The mixture was incubated for 24 hours at room temperature with shaking at 30 rpm on a Slow Speed Roto Mix (Barnstead Thermolyne). To remove free ELP, a 1 mL aliquot was transferred to a 50-kDa cutoff, 10 nm pore size, Float-A-Lyzer (Repligen, Waltham, MA), a high-efficiency device for the dialysis of small volume samples. The sample was dialyzed twice against 300 mL of DI H₂O for 2 hours at room temperature, and a final round of dialysis was conducted overnight. The dialysis protocol removed 99.3% of the free protein from preparations of V96-Cys-decorated 60 nm AuNPs, and 99.5% of the free protein from preparations of V96-Cys-decorated 20 nm AuNPs (**Table S1**). Protein-decorated particles were stable for months of storage at 4°C (**Fig. S4**). For some experiments, free V96-Cys was added back to dialyzed solutions at the indicated final concentration using an 80 μM stock solution of protein. Samples

were vortexed for 20 seconds prior to characterization.

Analytical techniques

The transition temperature (T_t) of V96-Cys was determined by dynamic light scattering (DLS) on a ZetaSizer (Malvern Instruments). To this end, protein samples (1 mL at a concentration of 10 μ M in DI H₂O) were heated from 20°C to 40°C with a step size of 2°C and a 5 minutes holding time at each temperature. DLS was also used to determine the hydrodynamic diameter (D_h) of V96-Cys-decorated AuNP clusters at different temperatures. Samples (1 mL) consisting of non-dialyzed V96-Cys-decorated AuNP were incubated at 20° C or 40° C for 5 minutes before acquisition of DLS data, while samples (1mL) consisting dialyzed V96-Cys decorated AuNP and the indicated concentration of free V96-Cys were incubated at 20°C or 40°C for 10 minutes before acquisition of DLS data.

For UV-Vis characterization, samples (200 μ L) were loaded in a 96-well plate and spectra were collected from 300 to 800 nm on a BioTek Synergy LX Multi-Mode plate reader with a step size of 5 nm. The temperature was varied from 20°C to 40°C with a 5 minutes holding time for non-dialyzed sample and a 10 minutes holding time for dialyzed sample at each temperature, respectively.

Cargo Entrapment and Release

For Nile Red (NR) fluorescence assays, 5 μ L of a 500 μ g/mL stock solution of NR in acetone was added to 245 μ L of DI H₂O containing dialyzed V96-Cys-functionalized AuNP and the indicated concentration of free ELP. The mixture was vortexed for 20 seconds and aliquots (200 μ L) were loaded in a 96-well plate held at room temperature. Samples were excited at 560 nm and emission intensities were measured at 620 nm on a BioTek Synergy LX Multi-Mode plate reader. The plate was covered and heated to 40°C in the instrument. Emission spectra were recorded after 30 minutes. The amount of entrapped NR was calculated from the difference in emission intensities at the two temperatures using the calibration curve

of **Fig. S5**. Samples were next transferred to a Float-A-Lyzer and dialyzed twice for 2 hours and once overnight at 40° C against 100 mL of pre-heated DI H₂O to remove the free dye. The amount of NR released upon cluster deconstruction was determined after 10 minutes and overnight incubation at 20° C using the calibration curve of **Fig. S5**. We used our smallest clusters (those produced by adding 0.5 μM of V96-Cys to 20 nm ELP-decorated AuNP) to demonstrate that no material escaped during the 40° C dialysis step. To this end, we compared the amount of free protein present in the supernatant of ultracentrifuged (50,000g for 10 min) samples held at 20°C, to that present in the supernatant of ultracentrifuged samples that had been incubated at 40°C to induce coacervation, dialyzed overnight at the same temperature, and cooled at 20°C for 24h to deconstruct clusters and regenerate a mixture of free V96-Cys and ELP-coated AuNPs. There was no significant difference in the amount free protein in the two samples ($0.50 \pm 0.03 \mu\text{M}$ vs. $0.48 \pm 0.04 \mu\text{M}$), demonstrating that no loss of material was incurred during dialysis.

For tetracycline (TC) assays, 100 μL of a 100 μg/mL stock solution of TC in DI H₂O was mixed with 300 μL of DI H₂O containing dialyzed V96-Cys-decorated AuNP and the indicated concentration of free ELP at room temperature. The mixture was vortexed for 20 seconds and aliquots (200 μL) were transferred to a 96-well plate held at room temperature. UV-Vis samples were acquired in the 300 nm to 800 nm window with a 1 nm step size. The plate was heated to 40°C in the instrument and UV-Vis spectra were recorded after 30 minutes. The amount of entrapped TC was calculated from the difference in absorbance at 356 nm at the two temperatures using the calibration curve of **Fig. S6**. Samples were extensively dialyzed at 40°C against 150 mL of DI H₂O as described for NR to remove free TC. The amount of TC released upon cluster deconstruction was measured after 10 minutes and overnight incubation at 20°C using the calibration curve of **Fig. S6**.

For scanning electron microscopy (SEM) imaging, aliquots (10 μ L) were deposited on silicon wafers and allowed to air dry overnight. For experiments conducted above T_t , sample wafers were pre-heated to 40°C and allowed to air dry overnight in an incubator held at the same temperature. Images were acquired on an Apreo-S SEM (Thermo Scientific) operated at 2 kV and 13 pA.

Growth Inhibition Experiments

We tested several common *E. coli* K-12 strains for TC sensitivity in the 0.25 to 5 μ g/mL range and selected HB101 (F^- *thi-1 hsdS20* (r_B^- , m_B^-) *supE44 recA13 ara-14 leuB6 proA2 lacY1 galK2 rpsL20* (*str^r*) *xyI-5 mtl-1*) as an adequately responsive strain. Overnight cultures (5 mL) grown at 37°C in LB broth were used to inoculate culture tubes containing 5 mL of fresh LB at a 1:50 dilution. Half of the tubes received increasing concentrations of TC in the 0.25 to 2.5 μ g/ml range from a 100 μ g/mL stock solution of the antibiotic. The other half were supplemented at a 1:50 dilution with TC entrapped in size-defined coacervates of V96-Cys-functionalized AuNPs produced at 40°C with various concentrations of free V96-Cys. Cultures were grown with shaking at 100 rpm for 48 hours at 20°C to induce TC release from the coacervates and the degree of growth inhibition was assessed by measuring culture optical density at 600 nm (A_{600}). Experiments were conducted in duplicate with no significant difference between samples.

RESULTS AND DISCUSSION

Thermoreversible Assembly of AuNP with a Gold-Binding ELP. To create an Au-binding ELP, we used site-directed mutagenesis to convert a Tyr residue at the C-terminus of a 96-repeat of the VPGVG sequence⁴⁶ to a Cys. The substitution had little effect on LCST behavior (**Fig. 1A**). The resulting protein (V96-Cys) experienced a sharp transition from unimers with a hydrodynamic diameter

(D_h) of 10.5 ± 1 nm at 20°C to 1050 ± 30 nm coacervates at a transition temperature (T_t) of 32°C that was comparable to that of the parental protein ($T_t = 31.9^\circ\text{C}$).⁴⁶

We next verified that the engineered C-terminal Cys would mediate coordination to gold interfaces by mixing citrate-capped 60 nm AuNP ($D_h = 64 \pm 5$ nm, **Fig. 1B**) with $13.3 \mu\text{M}$ of purified V96-Cys. This protein concentration was chosen to maintain colloidal stability during the ligand exchange step (**Fig. S3**). Dynamic light scattering (DLS) measurements conducted at 20°C revealed efficient formation of 115 ± 4 nm species consistent with AuNP surrounded by an about 25 nm protein shell (**Fig. 1B**). SEM imaging confirmed that V96-Cys-functionalized AuNP particles were well dispersed and featured a uniform protein coating that was 12 ± 1 nm ($N = 60$) thick under dry conditions (**Fig. 1C** and its inset).

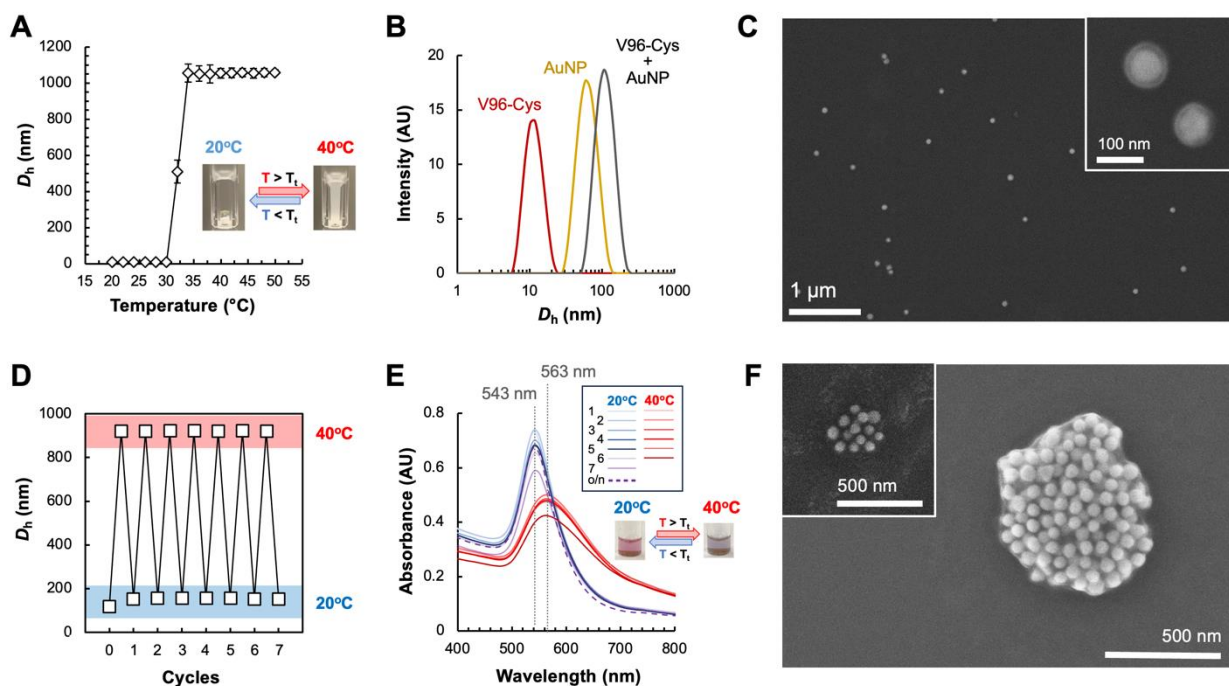


Figure 1 (A) DLS measurements show that V96-Cys rapidly transitions from 10 nm unimers to 1050 nm coacervates above a LCST of 32°C . The inset shows the appearance of a V96-Cys solution at 20°C and 40°C . (B) Size distributions of V96-Cys unimers, 60 nm AuNP, and V96-Cys-decorated AuNP particles at 20°C . (C) SEM image of V96-Cys-decorated AuNP at 20°C . The inset is a higher magnification image showing the ELP shell surrounding AuNPs. (D) Mean hydrodynamic diameter, and (E) UV-visible spectra of V96-Cys-decorated AuNPs over repeated cycles of heating and cooling between 20°C and 40°C . The inset in panel (E) shows the appearance of the solution at the two temperatures. (F) SEM image of a typical AuNP cluster assembled via V96-Cys coacervation at 40°C . The inset shows that smaller clusters comprising fewer AuNPs are also present in solution.

To determine if the ELP shell would mediate AuNP clustering above T_t and to test the thermoresponsiveness of the system, we repeatedly cycled samples between 20°C and 40°C, using DLS to monitor the change in size distributions after 5 min of equilibration at each temperature. **Fig. 1D** shows the exceptional reversibility of the transition between protein-decorated AuNPs with a mean D_h of 150 ± 3 nm and a polydispersity index (PDI) of 0.085 at 20°C, to clusters with a mean D_h of 926 ± 4 nm, but a higher PDI of 0.23 at 40°C. There was a small increase in the size of the ELP-decorated AuNP at the conclusion of the first temperature cycle that we attribute to the reconstruction of the protein shell after an initial round of coacervation-driven aggregation. UV-visible spectra collected after each heating and cooling step (**Fig. 1E**) showed that the transition from dispersed particles to aggregates was accompanied by a reversible 20 nm redshift in the localized surface plasmon resonance (LSPR) maximum.

To better understand the nature of this coupling and ascertain size distributions, we collected SEM images of aggregates formed at 40°C. The dry clusters had a mean diameter of 520 ± 31 nm ($N = 10$) that is consistent with the mean D_h of ~ 925 nm obtained by DLS. However, and in agreement with the PDI of 0.23 which is on the higher end of the monodisperse population cutoff, some clusters contained as few as a dozen AuNP that were well separated in an ELP matrix (**Fig. 1F**, inset), while others incorporated a larger number of AuNP and ranged in (dry) size from 320 to 540 nm (**Fig. 1F**; also see **Fig. S7**). Considering the sharp dependency of metal nanoparticle plasmonic coupling on separation distance,^{49,50} it is likely that the redshift observed in **Fig. 1E** originates from the large aggregates where AuNP have a greater chance of coming into close contact because they are not fully enveloped by an ELP layer.

Finally, there was a progressive decrease in the maximum intensity of the 543 nm (20°C) and 563

nm (40°C) peaks as the solution was cycled between the two temperatures (**Fig. 1E**). Because overnight incubation of the 20°C products obtained after seven cycles of temperature switching brings about a 15% increase in scattering intensity at 543 nm (dashed purple line in **Fig. 1E**), we attribute this phenomenon to insufficient equilibration time at 20°C for the full resolution of coacervates into protein-coated nanoparticles. Indeed, SEM imaging of samples collected at intermediate cycles of heating and cooling revealed that small clusters consisting of 2 to 8 AuNPs connected by ELPs persisted after 5 minutes of incubation at 20°C (**Fig. S8**).

In summary, V96-Cys efficiently coordinates gold to reversibly assemble AuNP with the advantages over PNIPAm of being monodispersed, genetically modifiable and biologically produced. Our results also show that although heating above T_t produces AuNP-loaded coacervates with a mean D_h of ~925 nm and a polydispersity index that is routinely associated with monodisperse populations, clusters sample a broad range of sizes.

Free ELP Controls the Size and Plasmonic Response of V96-Cys-Functionalized AuNP Assemblies. Based on the work of Jones *et al.*⁴⁵ who reported that full depletion of the free PNIPAm present in solutions of PNIPAm-decorated AuNPs precludes polymer-driven particle aggregation above the LCST, we set out to examine the role of free V96-Cys in AuNP assembly. To this end, we subjected 60 nm AuNP supplemented with an excess (13.3 μ M) of V96-Cys as above to extensive dialysis at 20°C before incubating the samples at 40°C. Unlike with the PNIPAm-AuNP system where no assembly was detected,⁴⁵ we reproducibly observed the formation of small clusters (D_h ~200 nm) that could be repeatedly dispersed and re-assembled by temperature cycling (**Fig. 2A** and **Fig. S9**). We attribute the formation of these clusters to the coacervation of a small number of ELP-decorated AuNPs by trace amounts of free V96-Cys. Indeed, **Table S1** shows that although dialysis removes over 99% of the free

V96-Cys in solution, about 70 nM of the protein persists in the samples. The same concentration of PNIPAm is sufficient to cause a small amount of clustering in the PNIPAm-AuNP system.⁴⁵

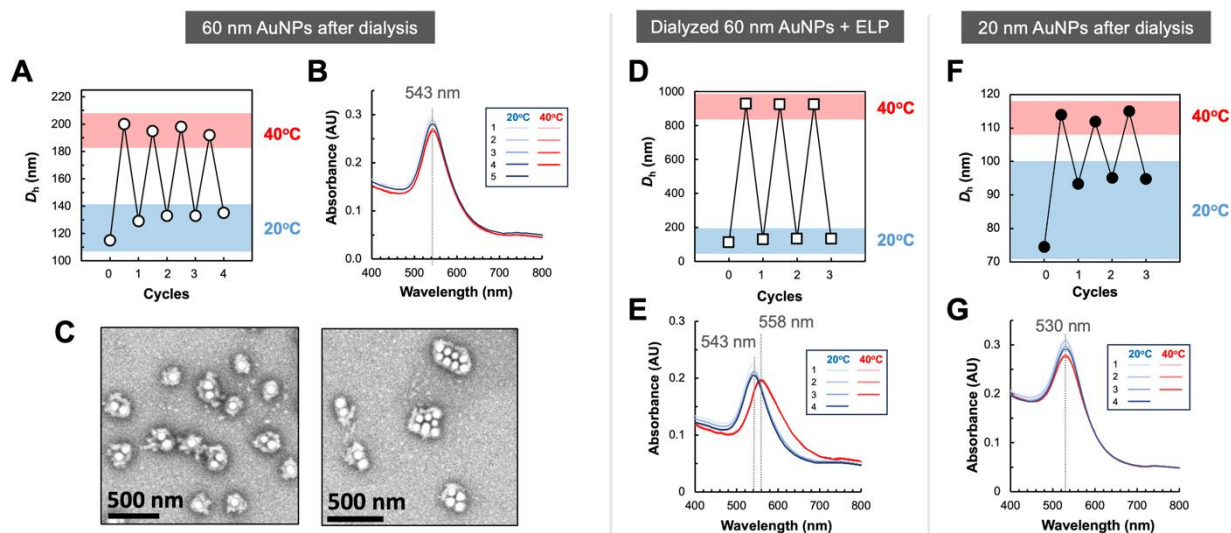


Figure 2 (A) Mean hydrodynamic diameters and (B) UV-visible spectra of extensively dialyzed V96-Cys-decorated AuNPs (60 nm) over repeated cycles of heating and cooling between 20°C and 40°C. (C) Representative SEM images of the ~200 nm AuNP-loaded coacervates produced at 40°C. Images were collected in backscattered electron mode to enhance contrast. (D) Mean D_h and (E) UV-visible spectra of the same particles after addition of an excess (13.3 μ M) of V96-Cys to the solution and repeated cycles of heating and cooling. (F) Mean D_h and (G) UV-visible spectra of extensively dialyzed V96-Cys-decorated AuNPs (20 nm) over repeated cycles of heating and cooling between 20°C and 40°C.

As in **Fig. 1D**, a reconstruction event increased the thickness of the ELP shell surrounding each particle by about 10 nm (to ~35 nm) after the first cycle of thermocycling. This did not impact the size of the clusters produced at 40°C (**Fig. 2A**), but there no longer was a shift in the LSPR maximum (**Fig. 2B**). Considering that the distance at which interparticle plasmonic coupling ceases can be coarsely taken as a half the AuNP diameter,^{51,52} we estimate that the interstitial protein layer separating coacervated AuNPs is at least 30 nm thick. Indeed, SEM imaging confirmed an enrichment in clusters made up of 2 to 8 AuNPs encased within a continuous ELP matrix (**Fig. 2C**, also see **Fig. S10**)

To confirm that the decrease in cluster size from 920 nm to 200 nm was caused by the removal of free ELP, we approximated the experimental conditions of **Fig. 1D** by supplying a dialyzed solution of

V96-Cys-functionalized AuNPs with 13.3 μM of ELP. Incubation at 40°C induced the formation of aggregates that were comparable in size ($D_h = 930$ nm) to those obtained with the original system (**Fig. 1D**). Furthermore, plasmonic coupling was restored, albeit with a slightly reduced (15 nm) redshift (**Fig. 2E**).

We next used 20 nm AuNPs to generalize results while probing the influence of surface curvature. As with larger AuNPs, incubation with excess V96-Cys caused particle functionalization with a 25 nm-thick protein shell ($D_h = 74 \pm 3$ nm, **Fig. S2**), temperature cycling between 20 and 40°C led to reversible formation and deconstruction of 930 ± 52 nm clusters (**Fig. S11A**), and coacervation was accompanied by a reversible ~ 20 nm redshift in the LSPR maximum (**Fig. S11B**). Additionally, removal of 99.5% of free V96-Cys by dialysis abrogated the formation of the 930 nm aggregates in favor of small clusters ($D_h = 115$ nm; **Fig. 2F** and **Table S2**) that no longer experienced plasmonic coupling (**Fig. 2G**). Of note, the first round of high temperature incubation also increased the thickness of the ELP shell by about 10 nm (**Fig. 2F**). In short, particle curvature appears to have little influence on coacervation-induced AuNP clustering as 20 nm V96-Cys-functionalized AuNPs behave like their 60 nm counterparts, except that the clusters they form above T_i after dialysis are about half the size of those produced with 60 nm AuNPs.

Precision Loading and Delivery of Molecular Cargos. Next, we explored if mean cluster size could be controlled by exogenous ELP addition. To this end, we supplied dialyzed, V96-Cys-decorated AuNPs with increasing concentrations of free protein and raised the temperature to 40°C before collecting DLS data. Addition of as little as 100 nM of V96-Cys to dialyzed solutions of 60 nm ELP-decorated AuNP increased the size of the clusters by over 2.5-fold (**Fig. 3A**). After this sharp increase in D_h , clusters progressively grew from 520 to 930 nm as the concentration of free V96-Cys was raised from 250 nM to 3 μM (**Table 1**). Importantly, polydispersity was very low as evidenced by narrow full

width at half maximum (FWHM) values for the size distributions (gray bars in **Fig. 3A**), DLS intensity profiles featuring a single peak (**Fig. S12**), and a PDI below 0.1 for clusters in the 520-870 nm size range (**Table 1**). Also of note, plasmonic coupling was restored upon addition of 250 nM V96-Cys, and both redshift and scattering intensity increased with the concentration of free ELP supplied (**Fig. S13**). This suggests that the number of AuNPs that are close enough to experience electromagnetic coupling (i.e., those not separated by an ELP layer) increases with cluster size. In the future, such defective particle envelopment and the associated redshift may prove useful to estimate cluster size by UV-visible spectroscopy, and to track individual clusters in complex environments with hyperspectral microscopy.

We obtained similar results – and accessed a smaller size range of 250 to 400 nm – by supplementing dialyzed solutions of V96-Cys-decorated 20 nm AuNPs with free ELP and inducing coacervation at 40°C (**Fig. 3B** and **Fig. S14**). While these clusters still qualify as monodisperse, their PDI values were larger (~0.2; **Table S2**). Finally, coacervation of free V96-Cys over the same range of

Table. 1 Mean hydrodynamic diameters and polydispersity indices of clusters formed by adding the indicated concentration of V96-Cys to dialyzed V96-Cys-functionalized AuNP (60 nm) and incubated the solution at 40°C.

Free V96-Cys (μM)	Mean D_h at 40°C (nm)	PDI
0	200	0.17
0.1	520	0.045
0.25	560	0.039
0.5	600	0.045
1	715	0.032
1.5	770	0.067
2	870	0.080
3	930	0.12

concentrations only yielded ~900 nm aggregates (**Fig. 3C**).

To determine if the formation of such size-controlled clusters could be exploited to load and release precise amounts of molecular cargo, we repeated experiments in the presence of 10 $\mu\text{g/mL}$ of Nile Red (NR), a lipophilic fluorescent dye. **Fig. 3D** shows that the amount of NR partitioning within clusters produced with 60 nm AuNP increased from 4.5 $\mu\text{g/mL}$ at a free V96-Cys concentration of 0.5 μM , to about 6.5 $\mu\text{g/mL}$ in the presence of 3 μM V96-Cys (pink bars). The dynamic range was even larger

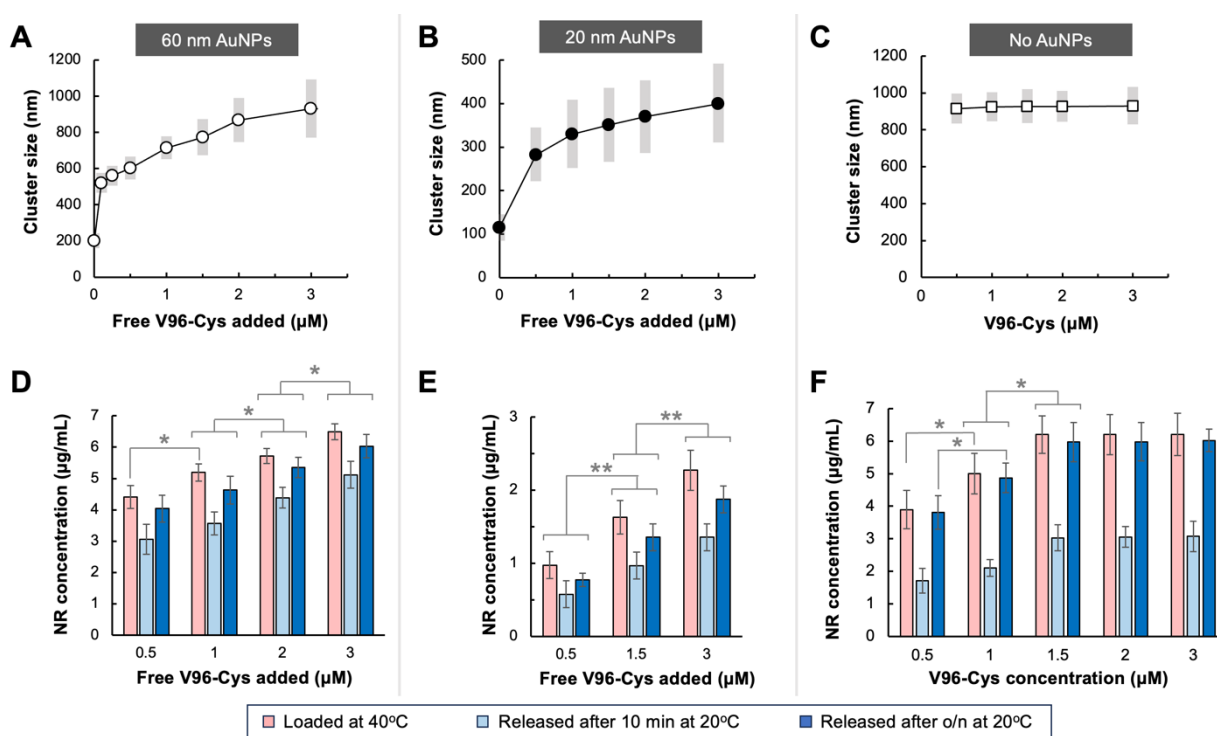


Figure 3 *Top panels:* Mean hydrodynamic diameters of AuNP-loaded coacervates (clusters) produced by incubating dialyzed, V96-Cys-decorated AuNPs 60 nm (A), or 20 nm (B) in size with the indicated concentrations of free V96-Cys at 40°C. (C) No size control is observed in the absence of AuNPs. Bars correspond to the full width at half maximum (FWHM) of the size distributions. *Bottom panels:* Quantification of the amount of Nile Red (NR) entrapped within size-controlled clusters produced by adding the indicated concentrations of free V96-Cys to V96-Cys-decorated AuNPs 60 nm (D), or 20 nm (E) in diameter, and incubating the mixture at 40°C (pink bars). (F) Entrapment of NR within coacervates formed by incubating the indicated concentrations of free V96-Cys at 40°C. NR was added at a concentration of 10 $\mu\text{g/mL}$ to all solutions prior to temperature upshift. Unincorporated NR was removed by dialysis at 40°C as described in Experimental Methods. NR release was measured after 10 min (light blue bars), or 24h of incubation at 20°C (dark blue bars). Error bars correspond to the root mean square deviation (RMSD) of two independent experiment. Significant differences between measurements are indicated (* $p < 0.05$ and ** $p < 0.01$).

when using 20 nm AuNPs (from 1 to 2.5 $\mu\text{g/mL}$ of loaded NR; **Fig. 3E**).

We next removed unincorporated NR by conducting dialysis at 40°C and transferred the samples to 20°C to induce cluster deconstruction. After 10 min of incubation, 70-80% of the NR associated with clusters formed with 60 nm AuNPs, and 60% of the NR uptaken by clusters produced with 20 nm AuNPs, had been released in solution (**Fig. 3D-E**, light blue bars). Overnight incubation at 20°C led to the release of an additional 10% (60 nm AuNPs) and 20% (20 nm AuNPs) of the cargo (**Fig. 3C-D**, dark blue bars). Thus, while most of the NR is rapidly released upon temperature downshift, a small amount appears to experience prolonged association with V96-Cys conformers that require time to return to their fully solvated, random coil conformation.

Although some degree of control could be exerted over the uptake and release of NR through the reversible coacervation of V96-Cys alone (**Fig. 3F**), there were significant differences relative to the AuNP system. First, control over NR loading was only possible over the 0.5 μM to 1.5 μM range of V96-Cys concentrations, and it was achieved more coarsely than when 60 nm ELP-decorated AuNPs were combined with 0.5 μM to 3 μM of free protein (**Fig. 3D**). Second, NR entrapment through free ELP coacervation did not allow access to the low NR loadings achieved with 20 nm AuNPs (**Fig. 3E**). Third, the entrapped NR was released more slowly from coacervates produced with free protein alone compared to those formed in the presence of ELP-decorated AuNPs (compare light blue bars in **Fig. 3D-F**).

To show that these observations reflect a fundamental difference in the mechanisms of cargo loading and release, we used confocal fluorescence microscopy to image NR-loaded coacervates produced with 3 μM of free V96-Cys or by adding the same concentration of protein to ELP-decorated 60 nm AuNPs. **Fig. S15** shows that the coacervates obtained with free V96-Cys alone were more polydisperse and less evenly loaded with NR compared to the clusters produced in the presence of

AuNPs.

Taken together, our data suggest that ELP-decorated AuNPs enable the production of clusters of defined sizes by serving as seeds that mediate the uniform consumption of bridging V96-Cys molecules until they are locally depleted and accretion ceases. This orchestrated growth process results in the production of rather monodisperse AuNP-loaded coacervates and explains the homogeneous incorporation of the surrounding NR cargo (and of its release during cluster deconstruction). By contrast, pure ELP alone forms coacervates through a random nucleation process that leads to heterogeneity in both coacervate size and cargo entrapment and release. Accordingly, the control of NR loading by V96-Cys in the 0.5-1.5 μM range is solely due to increased NR uptake by more numerous (or larger) aggregates. Why such uptake control ceases above 1.5 μM V96-Cys is less clear but may be related to a fine balance between the kinetics of coacervation and the depletion of the cargo in the vicinity of the growing coacervates.

Tetracycline (TC) is a broad-spectrum antibiotic that binds to a highly conserved region of the 16S RNA in the 30S ribosomal subunit of gram-positive and gram-negative bacteria to sterically interfere with protein elongation. The antibiotic is bacteriostatic (e.g., it blocks cell growth rather than killing pathogens) and some of its synthetic derivatives have shown potential for the treatment of multidrug-resistant pathogens in oral and intravenous delivery schemes.⁵³ TCs are also hydrophobic and various schemes (e.g., micelle-based formulations)⁵⁴ have been explored to enhance their bioavailability.

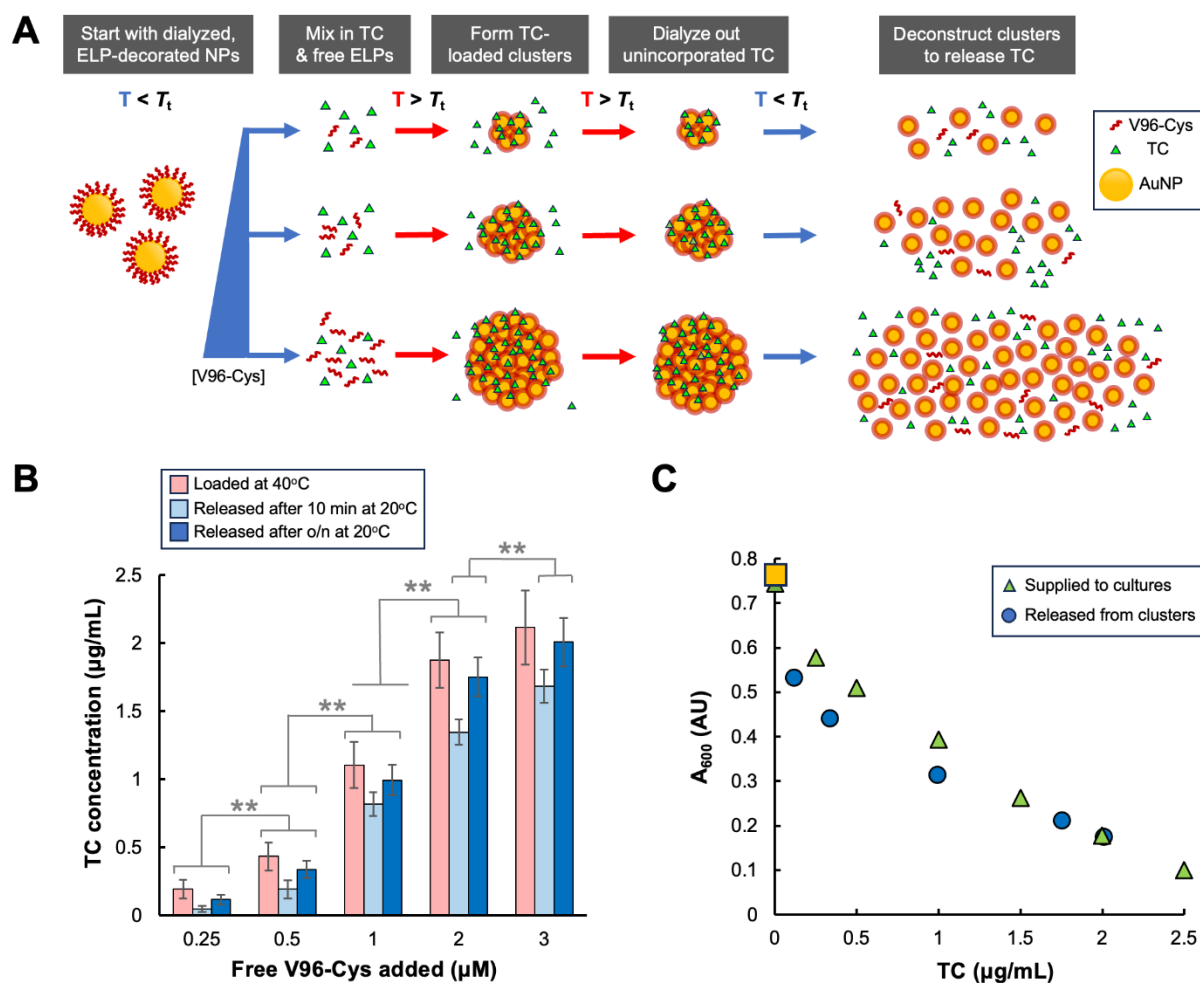


Figure 4 (A) Schematic illustration of the process used to load and release tetracycline (TC) in size-controlled, thermoresponsive clusters. (B) Quantification of the amount of TC loaded at 40°C (pink bars) and released from size-controlled clusters obtained with 60 nm AuNPs after 10 min (light blue bars), or 24h of incubation at 20°C (dark blue bars). Clusters were produced by incubating dialyzed V96-Cys-decorated AuNPs with 25 µg/mL of TC and the indicated concentration of free V96-Cys at 40°C. Significant differences between measurements are indicated (** $p < 0.01$). (C) Absorbance at 600 nm (A_{600}) of *E. coli* HB101 cultures supplemented with the indicated concentrations of TC through direct drug addition (green triangles), or temperature-induced deconstruction of clusters loaded with the indicated amount of TC after 48h of incubation at 20°C. The yellow square shows the A_{600} of untreated cultures. Experiments were repeated twice with synchronized cultures with no statistically significant differences in A_{600} values. Addition of AuNP alone or 3 µM of V96-Cys to the cultures caused no detectable growth inhibition.

We used TC and learnings from NR experiments to demonstrate a generic scheme for loading and delivering hydrophobic drugs *via* size-controlled, thermoresponsive clusters produced with 60 nm AuNPs (Fig. 4A). While TC uptake was low under our unoptimized experimental conditions, we achieved anFig. 4b order of magnitude dynamic range in drug entrapment by varying the concentration

of free V96-Cys from 250 nM to 3 μ M (**Fig. 4B**, pink bars). As was the case with NR, 10 minutes at 20°C was insufficient to fully release the entrapped cargo. However, TC release was nearly quantitative after 24h of incubation (**Fig. 4B**, light and dark blue bars). To confirm that the antibiotic was delivered in a dose-dependent and bioavailable manner, we mixed clusters produced at different concentrations of free ELP at 40°C with growth medium inoculated with *E. coli* HB101 cells. These cells are sensitive to the presence of TC in the concentration range that is relevant for our experiments (**Fig. S16A**). Samples were transferred to 20°C to induce cluster deconstruction and trigger antibiotic release, and the optical density of the cultures was measured at 600 nm (A_{600}) after 48 hours of cultivation to quantify the extent of growth inhibition. Consistent with our expectations, cell growth became poorer as the size of the provided clusters increased (**Fig. 4C and Fig. S16B**). Importantly, there was excellent agreement in the A_{600} values of cultures that had received TC through cluster deconstruction (TC concentration was determined from the data in **Fig. 4B**) and those that were directly supplied with increasing concentrations of the drug (**Fig. 4C**, compare blue circles to green triangles). We attribute the small differences in A_{600} at $TC \leq 1 \mu\text{g/mL}$ to the fact that the drug is immediately available for cellular uptake when it is directly added to the cultures.

CONCLUSION

We have shown here that, like PNIPAm-functionalized AuNPs,⁴⁵ ELP-decorated AuNPs require that free unimers be present in solution to undergo significant coacervation-induced aggregation above T_i . We have further demonstrated that the mean D_h of the clusters produced upon temperature upshift can be tuned in the 300 to 900 nm range – and their LSPR maximum progressively shifted to the red -- by specifying the amount of free V96-Cys that is added to dialyzed, protein-functionalized particles, and

by making use of AuNPs of different diameters. Finally, we have shown that precise amounts of hydrophobic molecular cargos, Nile red and tetracycline, can be homogeneously encapsulated within these size-controlled clusters during the coacervation process, and subsequently released during their deconstruction below T_t .

This simple approach to the production of monodisperse AuNP aggregates that are readily deconstructed by temperature downshift might prove useful for drug delivery and combination photothermal therapy or theranostics applications. Rapid release of discrete amounts of cargo from size-controlled clusters should also be useful to trigger spatially and temporally uniform responses from biological, electronic, or optical systems. Additionally, it should be straightforward to tune the T_t by manipulating the number of pentapeptide repeats, and to optimize the loading of specific cargos by changing the identity of the guest residue and/or the composition of the ELP sequence.^{55,56} Finally, it should be possible to expand the concept beyond AuNPs (e.g., to other metals, semiconductors, and oxides) by substituting a solid-binding peptide for the gold-coordinating Cys residue, and exploiting the binding and mineralizing properties of the resulting solid-binding ELP⁵⁷ to fabricate reconfigurable systems with applications in catalysis and opto-electronics.

ASSOCIATED CONTENT

Supporting Information

The Supporting Information is available free of charge at XXX

- Silver-stained SDS-PAGE gel analysis; Size distributions of V96-Cys unimers, 20 nm AuNP, and V96-Cys-decorated 20 nm AuNP at 20°C; UV-visible spectra of 60 nm AuNP supplied with/without indicated concentration of V96-Cys; SEM images of V96-Cys-decorated AuNP (60 nm) after 12 months of

storage at 4° C; Nile Red calibration curve; UV-visible spectra of Tetracycline and calibration curve; Additional SEM images of coacervates formed by V96-Cys-functionalized AuNP (60 nm) in the presence of 13.3 μM free ELP at 40°C; SEM images of V96-Cys-functionalized AuNP (60 nm) after 4 cycles of heating and cooling; Size distribution of dialyzed V96-Cys-decorated AuNPs (60 nm) at 20 and 40°C; Additional SEM images of coacervates formed by dialyzed, V96-Cys-functionalized AuNPs (60 nm) at 40°C; Size distribution and UV-visible spectra of V96-Cys-decorated 20 nm AuNPs over repeated cycles of heating and cooling; Size distributions of clusters formed by incubating dialyzed V96-Cys-functionalized AuNPs (60 nm) with free V96-Cys at 40°C; UV-visible spectra of dialyzed, V96-Cys-functionalized AuNPs (60 nm) supplemented with various amounts of free ELP at 20°C and 40°C; Size distributions of clusters formed by incubating dialyzed V96-Cys-functionalized AuNPs (20 nm) with free V96-Cys at 40°C; Confocal fluorescence images of Nile Red-containing V96-Cys coacervates produced by 3 μM pure V96-Cys or by mixing 3 μM of free protein with dialyzed V96-Cys-decorated AuNP (60 nm); Appearance of HB101 cultures supplied with increasing concentrations of TC or released TC via temperature-induced deconstruction of clusters; The dialysis protocol removes over 99% of the free protein from preparation of V96-Cys-decorated AuNPs; Mean D_h , FWHM, and PDI of clusters formed by V96-Cys-functionalized AuNP (20 nm) with various concentrations of free V96-Cys.

AUTHOR INFORMATION

Corresponding Author

*baneyx@uw.edu

ORCID

Notes

The authors declare no competing financial interest.

ACKNOWLEDGMENT

This material is based upon work supported by the US Department of Energy, Office of Science, Office of Basic Energy Sciences, as part of the Energy Frontier Research Centers program: CSSAS, The Center for the Science of Synthesis Across Scales under Award Number DE-SC0019288. SEM imaging was conducted at the University of Washington Molecular Analysis Facility, a member of the NSF National Nanotechnology Coordinated Infrastructure (NNCI).

REFERENCES

- (1) Wilson, W. M.; Stewart, J. W.; Mikkelsen, M. H. Surpassing Single Line Width Active Tuning with Photochromic Molecules Coupled to Plasmonic Nanoantennas. *Nano Lett.* **2018**, *18* (2), 853–858. <https://doi.org/10.1021/acs.nanolett.7b04109>.
- (2) Kundu, P. K.; Samanta, D.; Leizrowice, R.; Margulis, B.; Zhao, H.; Börner, M.; Udayabhaskararao, T.; Manna, D.; Klajn, R. Light-Controlled Self-Assembly of Non-Photoresponsive Nanoparticles. *Nat. Chem.* **2015**, *7* (8), 646–652. <https://doi.org/10.1038/nchem.2303>.
- (3) Sánchez-Moreno, P.; de Vicente, J.; Nardecchia, S.; Marchal, J. A.; Boulaiz, H. Thermo-Sensitive Nanomaterials: Recent Advance in Synthesis and Biomedical Applications. *Nanomaterials* **2018**, *8* (11), 935. <https://doi.org/10.3390/nano8110935>.
- (4) Karimi, M.; Sahandi Zangabad, P.; Ghasemi, A.; Amiri, M.; Bahrami, M.; Malekzad, H.; Ghahramanzadeh Asl, H.; Mahdih, Z.; Bozorgomid, M.; Ghasemi, A.; Rahmani Taji Boyuk, M. R.; Hamblin, M. R. Temperature-Responsive Smart Nanocarriers for Delivery Of Therapeutic Agents: Applications and Recent Advances. *ACS Appl. Mater. Interfaces* **2016**, *8* (33), 21107–21133. <https://doi.org/10.1021/acsami.6b00371>.
- (5) Wu, S.; Zhu, M.; Lian, Q.; Lu, D.; Spencer, B.; Adlam, D. J.; Hoyland, J. A.; Volk, K.; Karg, M.; Saunders, B. R. Plasmonic and Colloidal Stability Behaviours of Au-Acrylic Core–Shell Nanoparticles with Thin pH-Responsive Shells. *Nanoscale* **2018**, *10* (39), 18565–18575. <https://doi.org/10.1039/C8NR07440B>.
- (6) Palanikumar, L.; Al-Hosani, S.; Kalmouni, M.; Nguyen, V. P.; Ali, L.; Pasricha, R.; Barrera, F. N.; Magzoub, M. pH-Responsive High Stability Polymeric Nanoparticles for Targeted Delivery of Anticancer Therapeutics. *Commun. Biol.* **2020**, *3* (1), 1–17. <https://doi.org/10.1038/s42003-020-0817->

- 4.
- (7) Liu, Q.; Yuan, Y.; Smalyukh, I. I. Electrically and Optically Tunable Plasmonic Guest–Host Liquid Crystals with Long-Range Ordered Nanoparticles. *Nano Lett.* **2014**, *14* (7), 4071–4077. <https://doi.org/10.1021/nl501581y>.
 - (8) Kossyrev, P. A.; Yin, A.; Cloutier, S. G.; Cardimona, D. A.; Huang, D.; Alsing, P. M.; Xu, J. M. Electric Field Tuning of Plasmonic Response of Nanodot Array in Liquid Crystal Matrix. *Nano Lett.* **2005**, *5* (10), 1978–1981. <https://doi.org/10.1021/nl0513535>.
 - (9) Wang, M.; Gao, C.; He, L.; Lu, Q.; Zhang, J.; Tang, C.; Zorba, S.; Yin, Y. Magnetic Tuning of Plasmonic Excitation of Gold Nanorods. *J. Am. Chem. Soc.* **2013**, *135* (41), 15302–15305. <https://doi.org/10.1021/ja408289b>.
 - (10) Zheng, Y.; Soeriyadi, A. H.; Rosa, L.; Ng, S. H.; Bach, U.; Justin Gooding, J. Reversible Gating of Smart Plasmonic Molecular Traps Using Thermoresponsive Polymers for Single-Molecule Detection. *Nat. Commun.* **2015**, *6* (1), 8797. <https://doi.org/10.1038/ncomms9797>.
 - (11) Mayer, K. M.; Hafner, J. H. Localized Surface Plasmon Resonance Sensors. *Chem. Rev.* **2011**, *111* (6), 3828–3857. <https://doi.org/10.1021/cr100313v>.
 - (12) Astruc, D. Introduction: Nanoparticles in Catalysis. *Chem. Rev.* **2020**, *120* (2), 461–463. <https://doi.org/10.1021/acs.chemrev.8b00696>.
 - (13) Hubbell, J. A.; Chilkoti, A. Nanomaterials for Drug Delivery. *Science* **2012**, *337* (6092), 303–305. <https://doi.org/10.1126/science.1219657>.
 - (14) Mitchell, M. J.; Billingsley, M. M.; Haley, R. M.; Wechsler, M. E.; Peppas, N. A.; Langer, R. Engineering Precision Nanoparticles for Drug Delivery. *Nat. Rev. Drug Discov.* **2021**, *20* (2), 101–124. <https://doi.org/10.1038/s41573-020-0090-8>.
 - (15) Choe, A.; Yeom, J.; Shanker, R.; Kim, M. P.; Kang, S.; Ko, H. Stretchable and Wearable Colorimetric Patches Based on Thermoresponsive Plasmonic Microgels Embedded in a Hydrogel Film. *NPG Asia Mater.* **2018**, *10* (9), 912–922. <https://doi.org/10.1038/s41427-018-0086-6>.
 - (16) Carregal-Romero, S.; Buurma, N. J.; Pérez-Juste, J.; Liz-Marzán, L. M.; Hervés, P. Catalysis by Au@pNIPAM Nanocomposites: Effect of the Cross-Linking Density. *Chem. Mater.* **2010**, *22* (10), 3051–3059. <https://doi.org/10.1021/cm903261b>.
 - (17) Liu, W.; McDaniel, J.; Li, X.; Asai, D.; Quiroz, F. G.; Schaal, J.; Park, J. S.; Zalutsky, M.; Chilkoti, A. Brachytherapy Using Injectable Seeds That Are Self-Assembled from Genetically Encoded Polypeptides In Situ. *Cancer Res.* **2012**, *72* (22), 5956–5965. <https://doi.org/10.1158/0008-5472.CAN-12-2127>.
 - (18) Huang, X.; Jain, P. K.; El-Sayed, I. H.; El-Sayed, M. A. Plasmonic Photothermal Therapy (PPTT) Using Gold Nanoparticles. *Lasers Med. Sci.* **2008**, *23* (3), 217–228. <https://doi.org/10.1007/s10103-007-0470-x>.
 - (19) Salmaso, S.; Caliceti, P.; Amendola, V.; Meneghetti, M.; Magnusson, J. P.; Pasparakis, G.; Alexander, C. Cell Up-Take Control of Gold Nanoparticles Functionalized with a Thermoresponsive Polymer. *J. Mater. Chem.* **2009**, *19* (11), 1608–1615. <https://doi.org/10.1039/B816603J>.
 - (20) Mastrotto, F.; Caliceti, P.; Amendola, V.; Bersani, S.; Magnusson, J. P.; Meneghetti, M.; Mantovani, G.; Alexander, C.; Salmaso, S. Polymer Control of Ligand Display on Gold Nanoparticles for Multimodal Switchable Cell Targeting. *Chem. Commun.* **2011**, *47* (35), 9846–9848. <https://doi.org/10.1039/C1CC12654G>.
 - (21) Daniel, M.-C.; Astruc, D. Gold Nanoparticles: Assembly, Supramolecular Chemistry, Quantum-Size-Related Properties, and Applications toward Biology, Catalysis, and Nanotechnology. *Chem. Rev.* **2004**,

- 104 (1), 293–346. <https://doi.org/10.1021/cr030698+>.
- (22) Eustis, S.; El-Sayed, M. A. Why Gold Nanoparticles Are More Precious than Pretty Gold: Noble Metal Surface Plasmon Resonance and Its Enhancement of the Radiative and Nonradiative Properties of Nanocrystals of Different Shapes. *Chem. Soc. Rev.* **2006**, *35* (3), 209–217. <https://doi.org/10.1039/B514191E>.
- (23) Hostetler, M. J.; Templeton, A. C.; Murray, R. W. Dynamics of Place-Exchange Reactions on Monolayer-Protected Gold Cluster Molecules. *Langmuir* **1999**, *15* (11), 3782–3789. <https://doi.org/10.1021/la981598f>.
- (24) Schild, H. G. Poly(N-Isopropylacrylamide): Experiment, Theory and Application. *Prog. Polym. Sci.* **1992**, *17* (2), 163–249. [https://doi.org/10.1016/0079-6700\(92\)90023-R](https://doi.org/10.1016/0079-6700(92)90023-R).
- (25) Fujishige, S.; Kubota, K.; Ando, I. Phase Transition of Aqueous Solutions of Poly(N-Isopropylacrylamide) and Poly(N-Isopropylmethacrylamide). *J. Phys. Chem.* **1989**, *93* (8), 3311–3313. <https://doi.org/10.1021/j100345a085>.
- (26) Zhang, Y.; Furyk, S.; Bergbreiter, D. E.; Cremer, P. S. Specific Ion Effects on the Water Solubility of Macromolecules: PNIPAM and the Hofmeister Series. *J. Am. Chem. Soc.* **2005**, *127* (41), 14505–14510. <https://doi.org/10.1021/ja0546424>.
- (27) Du, H.; Wickramasinghe, R.; Qian, X. Effects of Salt on the Lower Critical Solution Temperature of Poly (N-Isopropylacrylamide). *J. Phys. Chem. B* **2010**, *114* (49), 16594–16604. <https://doi.org/10.1021/jp105652c>.
- (28) Foster, J. A.; Bruenger, E.; Gray, W. R.; Sandberg, L. B. Isolation and Amino Acid Sequences of Tropoelastin Peptides. *J. Biol. Chem.* **1973**, *248* (8), 2876–2879.
- (29) Urry, D. W.; Shaw, R. G.; Prasad, K. U. Polypentapeptide of Elastin: Temperature Dependence of Ellipticity and Correlation with Elastomeric Force. *Biochem. Biophys. Res. Commun.* **1985**, *130* (1), 50–57. [https://doi.org/10.1016/0006-291X\(85\)90380-8](https://doi.org/10.1016/0006-291X(85)90380-8).
- (30) Urry, D. W.; Luan, C. H.; Parker, T. M.; Gowda, D. C.; Prasad, K. U.; Reid, M. C.; Safavy, A. Temperature of Polypeptide Inverse Temperature Transition Depends on Mean Residue Hydrophobicity. *J. Am. Chem. Soc.* **1991**, *113* (11), 4346–4348. <https://doi.org/10.1021/ja00011a057>.
- (31) Urry, D. W.; Gowda, D. C.; Parker, T. M.; Luan, C.-H.; Reid, M. C.; Harris, C. M.; Pattanaik, A.; Harris, R. D. Hydrophobicity Scale for Proteins Based on Inverse Temperature Transitions. *Biopolymers* **1992**, *32* (9), 1243–1250. <https://doi.org/10.1002/bip.360320913>.
- (32) Urry, D. W. Physical Chemistry of Biological Free Energy Transduction As Demonstrated by Elastic Protein-Based Polymers. *J. Phys. Chem. B* **1997**, *101* (51), 11007–11028. <https://doi.org/10.1021/jp972167t>.
- (33) Meyer, D. E.; Chilkoti, A. Genetically Encoded Synthesis of Protein-Based Polymers with Precisely Specified Molecular Weight and Sequence by Recursive Directional Ligation: Examples from the Elastin-like Polypeptide System. *Biomacromolecules* **2002**, *3* (2), 357–367. <https://doi.org/10.1021/bm015630n>.
- (34) Meyer, D. E.; Chilkoti, A. Quantification of the Effects of Chain Length and Concentration on the Thermal Behavior of Elastin-like Polypeptides. *Biomacromolecules* **2004**, *5* (3), 846–851. <https://doi.org/10.1021/bm034215n>.
- (35) Nath, N.; Chilkoti, A. Interfacial Phase Transition of an Environmentally Responsive Elastin Biopolymer Adsorbed on Functionalized Gold Nanoparticles Studied by Colloidal Surface Plasmon Resonance. *J. Am. Chem. Soc.* **2001**, *123* (34), 8197–8202. <https://doi.org/10.1021/ja015585r>.
- (36) Alvarez-Rodriguez, R.; Alonso, M.; Girotti, A.; Reboto, V.; Rodriguez-Cabello, J. C. One-Pot

- Synthesis of pH and Temperature Sensitive Gold Clusters Mediated by a Recombinant Elastin-like Polymer. *Eur. Polym. J.* **2010**, *46* (4), 643–650. <https://doi.org/10.1016/j.eurpolymj.2009.12.022>.
- (37) Higashi, N.; Ochiai, T.; Kanazawa, C.; Koga, T. Site-Specific Adsorption of Gold Nanoparticles Coated with Thermo-Responsive Peptides. *Polym. J.* **2013**, *45* (5), 523–528. <https://doi.org/10.1038/pj.2012.220>.
- (38) Lin, Y.; Xia, X.; Wang, M.; Wang, Q.; An, B.; Tao, H.; Xu, Q.; Omenetto, F.; Kaplan, D. L. Genetically Programmable Thermo-responsive Plasmonic Gold/Silk-Elastin Protein Core/Shell Nanoparticles. *Langmuir* **2014**, *30* (15), 4406–4414. <https://doi.org/10.1021/la403559t>.
- (39) Ma, Q.; Liu, L.; Yang, Z.; Zheng, P. Facile Synthesis of Peptide-Conjugated Gold Nanoclusters with Different Lengths. *Nanomaterials* **2021**, *11* (11), 2932. <https://doi.org/10.3390/nano11112932>.
- (40) Huang, H.-C.; Koria, P.; Parker, S. M.; Selby, L.; Megeed, Z.; Rege, K. Optically Responsive Gold Nanorod–Polypeptide Assemblies. *Langmuir* **2008**, *24* (24), 14139–14144. <https://doi.org/10.1021/la802842k>.
- (41) Huang, H.-C.; Walker, C. R.; Nanda, A.; Rege, K. Laser Welding of Ruptured Intestinal Tissue Using Plasmonic Polypeptide Nanocomposite Solders. *ACS Nano* **2013**, *7* (4), 2988–2998. <https://doi.org/10.1021/nn303202k>.
- (42) Cheemalapati, S.; Ladanov, M.; Pang, B.; Yuan, Y.; Koria, P.; Xia, Y.; Pyayt, A. Dynamic Visualization of Photothermal Heating by Gold Nanocages Using Thermo-responsive Elastin like Polypeptides. *Nanoscale* **2016**, *8* (45), 18912–18920. <https://doi.org/10.1039/C6NR04676B>.
- (43) Kojima, C.; Fukushima, D. Applications of Gold Nanoparticle-Loaded Thermosensitive Elastin-Mimetic Dendrimer to Photothermal Therapy. *J. Photopolym. Sci. Technol.* **2016**, *29* (4), 519–523. <https://doi.org/10.2494/photopolymer.29.519>.
- (44) Sun, M.; Peng, D.; Hao, H.; Hu, J.; Wang, D.; Wang, K.; Liu, J.; Guo, X.; Wei, Y.; Gao, W. Thermally Triggered in Situ Assembly of Gold Nanoparticles for Cancer Multimodal Imaging and Photothermal Therapy. *ACS Appl. Mater. Interfaces* **2017**, *9* (12), 10453–10460. <https://doi.org/10.1021/acsami.6b16408>.
- (45) Jones, S. T.; Walsh-Korb, Z.; Barrow, S. J.; Henderson, S. L.; del Barrio, J.; Scherman, O. A. The Importance of Excess Poly(N-Isopropylacrylamide) for the Aggregation of Poly(N-Isopropylacrylamide)-Coated Gold Nanoparticles. *ACS Nano* **2016**, *10* (3), 3158–3165. <https://doi.org/10.1021/acsnano.5b04083>.
- (46) Shah, M.; Hsueh, P.-Y.; Sun, G.; Chang, H. Y.; Janib, S. M.; MacKay, J. A. Biodegradation of Elastin-like Polypeptide Nanoparticles. *Protein Sci.* **2012**, *21* (6), 743–750. <https://doi.org/10.1002/pro.2063>.
- (47) Meyer, D. E.; Chilkoti, A. Purification of Recombinant Proteins by Fusion with Thermally-Responsive Polypeptides. *Nat. Biotechnol.* **1999**, *17* (11), 1112–1115. <https://doi.org/10.1038/15100>.
- (48) Anthis, N. J.; Clore, G. M. Sequence-Specific Determination of Protein and Peptide Concentrations by Absorbance at 205 Nm. *Protein Sci. Publ. Protein Soc.* **2013**, *22* (6), 851–858. <https://doi.org/10.1002/pro.2253>.
- (49) Kelly, K. L.; Coronado, E.; Zhao, L. L.; Schatz, G. C. The Optical Properties of Metal Nanoparticles: The Influence of Size, Shape, and Dielectric Environment. *J. Phys. Chem. B* **2003**, *107* (3), 668–677. <https://doi.org/10.1021/jp026731y>.
- (50) Jain, P. K.; El-Sayed, M. A. Plasmonic Coupling in Noble Metal Nanostructures. *Chem. Phys. Lett.* **2010**, *487* (4), 153–164. <https://doi.org/10.1016/j.cplett.2010.01.062>.
- (51) Reinhard, B. M.; Siu, M.; Agarwal, H.; Alivisatos, A. P.; Liphardt, J. Calibration of Dynamic Molecular Rulers Based on Plasmon Coupling between Gold Nanoparticles. *Nano Lett.* **2005**, *5* (11), 2246–2252.

<https://doi.org/10.1021/nl051592s>.

- (52) Jain, P. K.; Huang, W.; El-Sayed, M. A. On the Universal Scaling Behavior of the Distance Decay of Plasmon Coupling in Metal Nanoparticle Pairs: A Plasmon Ruler Equation. *Nano Lett.* **2007**, *7* (7), 2080–2088. <https://doi.org/10.1021/nl071008a>.
- (53) Grossman, T. H. Tetracycline Antibiotics and Resistance. *Cold Spring Harb. Perspect. Med.* **2016**, *6* (4), a025387. <https://doi.org/10.1101/cshperspect.a025387>.
- (54) Meretoudi, A.; Banti, C. N.; Siafarika, P.; Kalampounias, A. G.; Hadjikakou, S. K. Tetracycline Water Soluble Formulations with Enhanced Antimicrobial Activity. *Antibiotics* **2020**, *9* (12), 845. <https://doi.org/10.3390/antibiotics9120845>.
- (55) Varanko, A. K.; Su, J. C.; Chilkoti, A. Elastin-Like Polypeptides for Biomedical Applications. *Annu. Rev. Biomed. Eng.* **2020**, *22* (1), 343–369. <https://doi.org/10.1146/annurev-bioeng-092419-061127>.
- (56) Guo, Y.; Liu, S.; Jing, D.; Liu, N.; Luo, X. The Construction of Elastin-like Polypeptides and Their Applications in Drug Delivery System and Tissue Repair. *J. Nanobiotechnology* **2023**, *21* (1), 418. <https://doi.org/10.1186/s12951-023-02184-8>.
- (57) Pushpavanam, K.; Ma, J.; Cai, Y.; Naser, N. Y.; Baneyx, F. Solid-Binding Proteins: Bridging Synthesis, Assembly, and Function in Hybrid and Hierarchical Materials Fabrication. *Annu. Rev. Chem. Biomol. Eng.* **2021**, *12* (1), 333–357. <https://doi.org/10.1146/annurev-chembioeng-102020-015923>.